Electron capture at low velocity in the collision of Ar17+ ions with atoms, clusters and solids

Christophe Prigent, E. Lamour, J. -P. Rozet, S. Steydli, Martino Trassinelli, Dominique Vernhet

Electron capture at low velocity in the collision of Ar^{17+} ions with atoms, clusters and solids

2014 J. Phys.: Conf. Ser. 488 012029

(http://iopscience.iop.org/1742-6596/488/1/012029)

Journal of Physics: Conference Series **488** (2014) 012029 doi:10.1088/1742-6596/488/1/012029

Electron capture at low velocity in the collision of Ar^{17+} ions with atoms, clusters and solids

C Prigent, E Lamour, J.-P. Rozet, S. Steydli, M. Trassinelli and D. Vernhet

Institut des Nanosciences de Paris, CNRS- UMR7588, Université Pierre et Marie Curie, Paris, France

E-mail: christophe.prigent@insp.jussieu.fr

Abstract. Absolute x-ray emission has been measured when Ar^{17+} ions at 255 keV collide either with atomic gaseous targets of Ar or N_2, with Ar clusters or with thin carbon foils. Preliminary results show a strong decrease of the x-ray signal with the backing pressure of the cluster supersonic jet compared to ion-atom interaction. This effect is a clear signature of slow highly charged ions interacting with clusters. Additionally, high resolution x-ray technique gives us access to the charge state distribution of the emitting ions.

1. Introduction

Interaction of slow Highly Charged Ions (HCI) with matter is of great interest in various fields as, for example, in astrophysical plasmas [1], in surface modifications [2, 3] or in capillary ion guiding [4]. In the low collision energy regime (below a few tens of keV/q), the dominant electronic process is the capture of target electrons by the HCIs. The basic processes are summarized hereinafter for two extreme cases of targets (atom and surface/solid). When considering an atomic target, the resonant capture of a single electron occurs in highly excited states of the projectile ions, i.e. in levels of high-*n* principal quantum number. The geometrical cross section, well predicted by the classical over-the-barrier model, is then found to be of the order of $0.5\times\pi\times R_c^2$ [5] where R_c is the capture radius. Multiple electron capture that populates efficiently lower *n* values takes place as well. This process starts to play an important role especially when using ions with a high q charge [6, 7], and obviously heavy atomic targets. Finally, the excited ion stabilizes *via* radiative decay and autoionization (Auger effect). With solid targets, many experiments [8, 9, 10, 11] have been carried out with ions directed at grazing or normal incidence onto the target to investigate the rapid neutralization (formation of hollow atoms of first generation) and charge equilibration (through relaxation processes) of HCIs near the surface. If the hollow projectile hits the surface, peel-off process (ejection of the most loosely bound electrons) takes place while side feeding mechanism [12] appears. This latter corresponds to a rapid inner shell transfer process (Auger neutralization between the target and the projectile) leading to a more compact hollow atom of second generation. When the projectile enters inside the solid, this process is then in time competition with the relaxation (radiative and Auger) effects of the ion [9, 13] through multiple step collisions. In both cases, i.e., either with atom [7, 14] or solid (bulk or surfaces) [15], x-ray spectroscopy techniques of excited states of HCIs formed by capture of target electrons have proved to be a very powerful tool to study the interaction dynamics. For instance, Briand *et al.* [15] demonstrate that the hollow atom clock property may be used to investigate continuously the approach and penetration of an ion onto a surface via the study of the *L*-shell filling in the case of

argon ions. Moreover, this shell filling has been shown to be also sensitive to the electronic structure of the solid (metal or insulator) [16].

Clusters bridge the gap between isolated atoms and solids. Depending on the ion impact parameter (b), the cluster size (R_{cl}) and the capture radius (R_c), HCI-cluster interaction is expected to behave like HCI-atom interaction for $b \geq R_{cl} + R_c$, HCI-surface interaction for $R_{cl} - R_c < b < R_{cl} + R_c$ or HCI-bulk interaction for $b \leq R_{cl} - R_c$. For instance, using the projectile energy-loss analysis, collision events have been successfully separated upon the impact parameters for slow Ne^{10+} colliding with C_{60} [17]. Obviously, the electronic structure of clusters will have impact as well on the observed features of the interaction. The electronic response of C_{60} and clusters of fullerenes have been widely studied. The high charge mobility found for clusters of fullerenes [18] is in contrast to charge localization effects which have been reported for small (a few atoms per cluster) ionized argon clusters [19]. There is still a lack of investigation for insulating clusters as rare gas clusters of van der Waals type and no x-ray measurements have been so far performed.

In this paper, we present new results on collisions of Ar^{17+} ions ($v = 0.53$ a.u., i.e. energy of 255 keV) with atomic gaseous targets (Ar and N_2), argon clusters of nanometer size and thin carbon foils of a few tens of nm. The 3-4 keV x-rays emitted by the projectile argon ions are carefully analyzed. With solid-state detectors, the x-ray emission probability is measured for all the target types. A Bragg crystal spectrometer enables us to determine the electronic structure of the excited states (np population or K^xL^y configuration) of emitting ions with a high resolution in the case of atoms and thin solids. When using a supersonic cluster jet, the total x-ray yield has been investigated as well. We will show that a reduction of the x-ray signal is observed when increasing the backing pressure P_0 in the cluster production system. It is worth mentioning that this behavior is in contrast with what happens in the case of HCI-atom interaction for which a linear-dependence is observed [14] when single collision condition is fulfilled. In other words, since when increasing P_0 (from 5 to 25 bar in our experimental conditions) the aggregation is favored, the reduction of the x-ray yield signs the presence of clusters in the jet.

2. Experimental set-up and detection system

The experiment, performed at the low energy installation ARIBE in Caen (French acronym for Accelerator dedicated to research with low energy ions), has already been described in details in [14 and 20]. Briefly summarized here, 255 keV Ar^{17+} ions from an ECR ion source are selected and directed onto a target located at the center of a collision chamber. The ion beam interacts with atomic or cluster targets at 90° of the propagation direction of the gaseous jet and at normal incidence for solid targets. A beam intensity of around 2 nA is measured by a Faraday cup installed just after the interaction zone. The x-rays emitted by the projectile ions during the interaction are recorded by means of two silicon drift detectors (SDD) placed respectively at 30° and 120° with respect to the ion beam axis and by a high transmission high resolution Bragg crystal spectrometer located at -30°. The SDDs, well calibrated in terms of energy and efficiency [21], record the complete series of x-ray transitions with an energy resolution of typically ~ 200 eV at 3 keV. To ensure a resolution of 3 eV at ~ 3 keV with the crystal spectrometer, the ion beam is vertically focused to 1-3 mm. The beam profile is then regularly checked detecting, with a high sensitivity CCD camera, the fluorescence light from the ion impact on a silicon or alumina target. It is worth mentioning that when a jet (atomic or cluster jet) is used as a target, the SDDs are equipped with long specifically designed collimators in which a diaphragm is inserted to get rid of background contribution.

3. Targets: production and characteristics

3.1. Atomic gaseous targets

For the production of isolated atoms, an effusive gas jet obtained by diffusion through a capillary of 3.5 cm length and 1 mm of diameter is used. Working in the so-called opaque intermediate regime [22, 23, 24], with a baking pressure in the capillary of typically 1.5 mbar, an atomic density at the

interaction zone of 5 10^{12} at/cm^3 is reached with a well defined spatial extension of 8 mm at 6 mm below the exit of the capillary. Under these conditions, we have checked that the single collision condition is fulfilled with pressures up to 3 mbar [14].
Argon and molecular nitrogen gases have been used. As expected, molecular nitrogen leads to very similar results compared to atomic argon target. Indeed, the typical capture radius, which is around $R_c \approx 7$Å from classical over-barrier predictions, is larger than the size of the bi-nitrogen (1 Å), and in both cases, six electrons are available in the highest lying states.

3.2. Thin solid targets

Thin solid foils of carbon are relatively easy to manufacture and to handle. The solid targets used are of amorphous type and are made by an evaporation technique on glass slides coated with a wetting (typically NaCl). The carbon film is then separated from the glass and collected on an aluminum support drilled with a hole of a large size (6 mm of height × 18 mm of length) with respect to the ion beam which is vertically focused to 1–3 mm and limited to a beam width of 10–15 mm. Two self-supported carbon foils with a thickness of 2 and 15.5 µg/cm² (i.e. 10 nm and 80 nm respectively) have been studied. Their atomic density is of 10^{23} at/cm^3 and they present a semi-metallic behavior with a gap that does not exceed 0.5 eV [25]. Let us note that they correspond to an atomic surface density of 10^{17} cm^{-2} and 8.10^{17} cm^{-2} respectively. The mean energy loss of the Ar projectiles when passing the carbon foils is of 13 keV with a mean scattering angle close to 3° for 10 nm and of 100 keV with a mean scattering angle of 10° for 80 nm. Those values are extracted from the SRIM code version 2008.04 [26] that gives reasonable predictions compared to experimental data [27, 28]).

3.3. Cluster source

To cover the gap between isolated atoms and solids, clusters are obviously good candidates since they offer the possibility to easily change the surface/volume ratio. Argon clusters, having an insulator behavior with a very high gap of 14.2 eV [29], are generated within a pulsed adiabatic expansion of a gas flow at high pressure (i.e., a baking pressure P_0 from a few to several tens of bar) through a conical nozzle of Hagena type [30] that opens into an expansion chamber maintained at a pressure much lower than P_0. The nozzle (length $L = 23$ mm and half opening angle $2\alpha = 7.5°$) is mounted on a solenoid pulsed valve operated at a repetition rate in the 1 - 20 Hz range and having a throat diameter (d) of either 300 µm or 100 µm. An opening duration of ~ 300 µs has been used. Between the expansion chamber of the cluster jet and the collision chamber, a skimmer with a diameter of 1 mm is used to select the coldest part of the cluster jet. The distance (z) between the nozzle and the collision zone may be varied over several cm. For a given geometry, i.e. for fixed parameters (L, α, d and z), the mean atomic density (n_{at}) of the cluster jet and the cluster size (the number of atoms per cluster $N_{at/cl}$) depend on the backing pressure P_0 as $n_{at.} \propto P_0$ and $N_{at./cl.} \propto P_0^2$ respectively. The clusters formed have local density close to the solid one (~ 10^{22} at/cm^3). With backing pressures from 5 to 25 bar and working at a distance z of 366 mm, we have measured mean atomic densities in the $10^{11} - 10^{12}$ at/cm^3 range thanks to energetic electron-cluster jet interaction experiments [31]. The cluster radius may reach a value of around 6 nm at the maximum P_0 value (i.e. for $P_0 = 25$ bar). Consequently, the energy loss of the incoming ions shall not exceed 2 keV in this case. Furthermore, we have to keep in mind that the cluster jet is, in fact, a mixture of free atoms and clusters.

4. X-ray emission probabilities per incoming ions and target atoms for gaseous and solid targets

Two low-resolution spectra recorded by one of the SDD are presented in Figure 1. With a gaseous jet (Figure 1-a), only He-like Ar^{16+} transitions are observed. Two major peaks are clearly visible in the energy region from 3 to 3.8 keV. As explained already in [14], they are assigned to the 1s2p→1s² (high intensity line) and 1s3p→1s² transitions. The broad peak at higher energy is due to 1snp→ 1s² transitions with $n > 3$. With a thin solid foil (Figure 1-b), the spectrum looks different: the peaks are shifted and present a net broadening characteristic of the Kα, Kβ, … lines in the 2.8-3.9 keV energy

region emitted by argon ions having different number of electrons in the L shell and, more or less, a full M shell.

In both cases, quantitative peak intensities (N_{np}) have been extracted by fitting the observed lines with a series of Gaussian profiles after background subtraction. The absolute total number of x-rays (N_x) reaching the detector is obtained by:

$$N_X = \sum_n \frac{N_{np}}{\varepsilon_{np}} \tag{1}$$

with ε_{np}, the detector efficiency at the energy of the *np* transition considered (for example ε=0.91±0.03 for the 2p1s→1s² transition around 3.1 keV).

As presented in [14], in the case of a gaseous target, the number of x-rays, N_x, that reaches the detector over an integration time *T* is linked to the absolute x-ray emission cross section σ_{x-ray} (in cm^2) via the beam – jet overlap integral according to the following formula :

$$\frac{N_X}{IT} = \sigma_{x-ray}.\left(B(p) + B_{res}(p)\right) \tag{2}$$

where *I* is the ion beam intensity (ions per second) and B(p), the beam – jet overlap integral given by Eq (1) in [14], $B_{res}(p)$ being the overlap integral of the ion beam with the residual gas inside the collision chamber over the entire zone viewed by the detector. The collimation system (long collimators and diaphragms), used in the case of gaseous jet, gives rise to an effective solid angle of $8\ 10^{-3}$ sr and $1.6\ 10^{-3}$ sr for the SDD placed at 30° and 120° respectively (including shadow effects and integrated over the whole beam-jet overlap). As reported in [14], we measure an absolute cross section of $11.4\ 10^{-15}$ cm² (± 15%) whatever the nature of the gas, i.e. argon atoms or molecular nitrogen.

In the case of a solid target, the number of x-rays, N_x, reaching the detector over an integration time *T* and normalized to the ion beam intensity, *I*, can be expressed as the product of the number of target atoms, N_{target}, and the x-ray emission probability $P_{x\text{-}ray,}$ using the following relation:

$$\frac{N_X}{IT} = P_{x-ray}.N_{target}.\frac{\omega}{4\pi} \tag{3}$$

where $\omega/4\pi$ is the solid angle. For the SDD placed at 30°, ω is $1.15\ 10^{-3}$ sr. This equation, valid for homogeneous targets, is formally identical to equation 2 that applies for an inhomogeneous gaseous target. If N_{target} is expressed in term of number of atoms per cm^2 (atomic surface density), $P_{x\text{-}ray}$ is then in cm^2, allowing a pertinent comparison with the x-ray emission cross section ($\sigma_{x\text{-}ray}$) obtained for the ion-atom interaction. For solid carbon foils, the x-ray emission probabilities (per incoming ions and target atoms) are found to be $2\ 10^{-19}$ cm² with the thinnest target (10 nm = 10^{17} at./cm^2) down to $1.7\ 10^{-20}$ cm² for the thickest target (80 nm = 8.10^{17} at./cm^2).

As the x-ray emission probability in the bulk is much smaller than the x-ray emission cross section with atoms ($P_x^{bulk} \sim 10^{-19}$ cm² << $\sigma_x^{atom} \sim 10^{-14}$ cm²), in the case of a cluster, the contribution of the x-ray emission from the bulk is negligible.

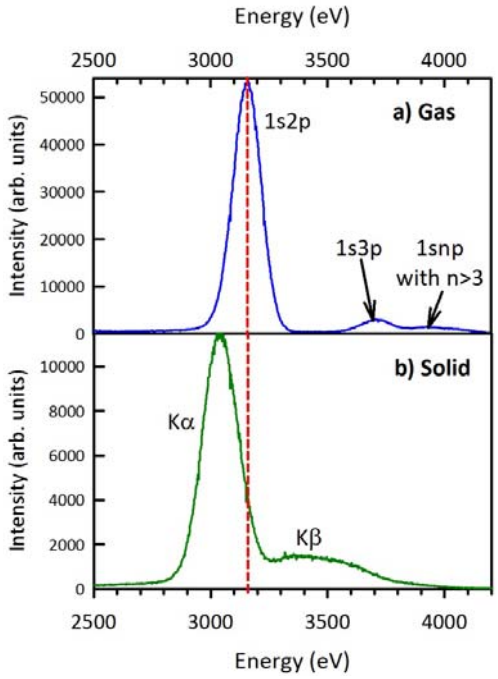

Figure 1. Low-resolution x-ray spectra obtained with one of the SDD when Ar^{17+} (v = 0.53 a.u.) ions collide either with (a) isolated atoms or (b) with a 80 nm carbon foil: (a) exhibits $1snp \rightarrow 1s^2$ Ar^{16+} transitions (the red vertical line indicates the position of the $1s2p \rightarrow 1s^2$ transition) while K x-ray transitions are visible on (b).

5. High resolution spectra for gaseous and solid targets

With the high-resolution spectrometer, an efficient zoom of the SDD spectra is achievable as shown in Figures 2 and 3. A record of the full x-ray series requires to set the spectrometer at a minimum of four different Bragg angles. The two figures obtained with a gaseous target (Figure 2) and a thin carbon foil (Figure 3) are plotted over the same energy range (2950 – 4125 eV) for comparison. With atoms, all the Ar^{16+} $1snp\ ^1P_1 \rightarrow 1s^2$ transitions with n from 2 to 10 are extremely well separated. At low energy, for $n = 2$ the $^{1,3}P$ states and the contribution from the $1s2s\ ^3S_1$ sub-level are also visible. A careful examination of the full spectrum has already brought noticeable results [14] and new benchmarks for full theoretical calculations [32]: the precise determination of the n-population probability for the single-electron capture in n = 7-10, the contribution of the multi-electron capture in lower n-values and a reliable measurement of the hardness ratio. Obviously, when compared with a thin solid foil (Figure 3), the spectrum is completely different. As it has been already observed by Briand *et al.* [15-16], the deexcitation from Ar K^1L^1 (Ar^{16+}-like) excited states has almost entirely disappeared while those from levels with more electrons in the L shell are clearly visible up to Ar K^1L^8. In more details, as the energy of the K x-ray depends on the number of electrons (x) present in the L shell, 8 $K^1L^x \rightarrow K^2L^{x-1}$ transitions are observed as shown in Figure 4 for which only the Kα line is plotted. The spectrum in Figure 3 is indeed the result of a complex competition between various processes, namely multistep capture, side feeding mechanisms and Auger/radiative effects [13]. No noticeable differences are observed when comparing the K^1L^x peak intensities obtained with the two different carbon thicknesses as illustrated in the inset of Figure 3. Consequently, the charge state equilibrium of the ion emitting an x-ray is already reached for the thinnest target as previously observed for similar experimental conditions in [28].

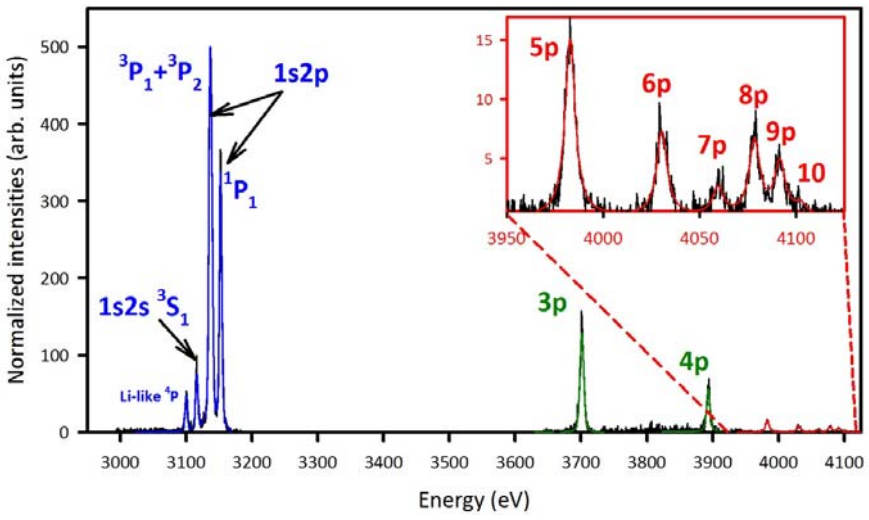

Figure 2. Full high-resolution spectrum of Ar^{16+} 1s*n*p→1s² transitions for Ar^{17+} at v = 0.53 a.u. on an atomic argon target (p = 1.5 mbar). Zoom of the end part of the spectrum is shown in the inset.

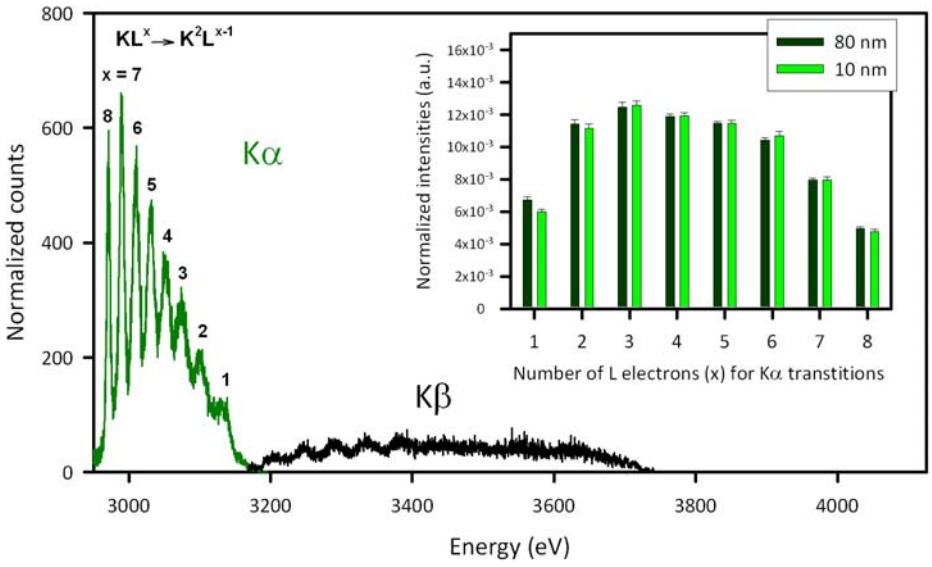

Figure 3. Full high-resolution spectrum exhibiting the structure of the Kα (see also Figure 4) and Kβ transitions for Ar^{17+} at 0.53 a.u. on a 80 nm carbon foil. In the inset, normalized intensities of the Kα lines from Ar K^1L^x with $1 \le x \le 8$ for two different target thicknesses.

We note that the relative intensity of the K^1L^x transitions depends on the electronic structure of the target. It turns out that the filling of the L shell is quasi completed with metallic targets in contrast to what happens with dielectrics [16]. As a result, the K^1L^8 transition dominates the spectrum with metals while the K^1L^x intensity distribution is rather peaked on K^1L^6 with insulators. Note that the spectrum obtained with a carbon foil is found to be intermediate between those two cases.

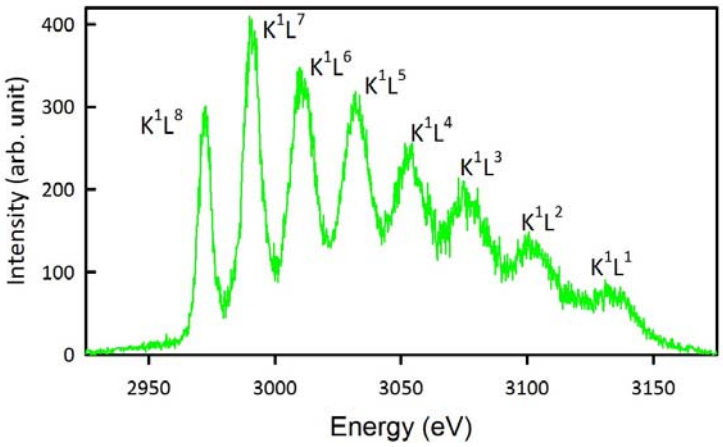

Figure 4. High resolution x-ray spectrum of the Kα line emitted when Ar^{17+} (v = 0.53 a.u.) ions collide with a 10 nm carbon foil: $K^1L^x \rightarrow K^2L^{x-1}$ transitions emitted by Ar^{q+} (with $1 \leq x \leq 8$) are clearly visible.

6. Total x-ray signal with the cluster jet

The low resolution x-ray spectra with the cluster jet look similar to Figure 1-a, i.e. to what is observed with the effusive jet. Nevertheless, we observe that the $np \rightarrow 1s/2p \rightarrow 1s$ intensity ratio (with $n \geq 3$) is significantly higher by around a factor of 2 when compared to Ar^{17+} ions colliding with an atomic Ar target. In terms of intensity, preliminary results show that the global x-ray signal decreases when increasing the backing pressure (P_0) as illustrated in Figure 5. This behavior is in contrast with the evolution observed with isolated atoms that exhibits a linear dependence with the pressure (Figure 6) when the single collision condition is fulfilled.

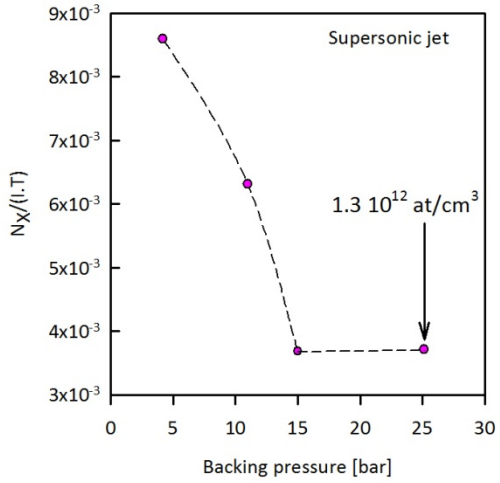

Figure 5. Evolution of the x-ray emission with the backing pressure of the argon cluster jet (preliminary results obtained with the throat diameter of 100 µm). The dashed line is to guide the eyes and the arrow indicates the total atomic density at 25 bar.

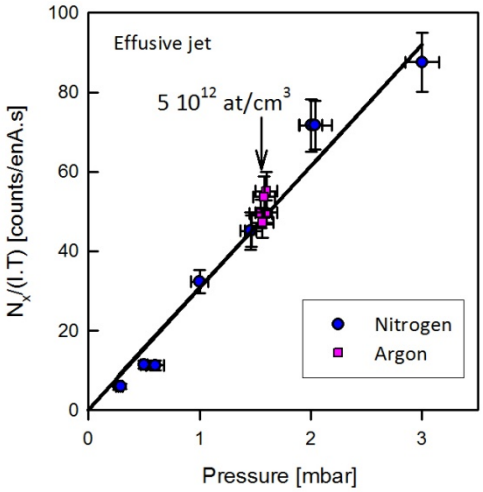

Figure 6. Evolution of the x-ray emission with the pressure of the gaseous jet for N_2 and Ar. The solid line corresponds to Equation 3 in [14]. The arrow indicates the total atomic density at 1.5 mbar.

Nevertheless this trend can be well understood. Indeed, at this stage, one can assume the capture cross section for clusters to be of the same order of magnitude than for isolated atoms. Furthermore, in a supersonic jet, the cluster density ($\propto 1/P_0$) is much lower than the density of free atoms ($\propto P_0$) by

several orders of magnitude [31]. Consequently the x-ray emission is mainly coming from the free remaining atoms in the gaseous bunch but which decreases dramatically with the backing pressure since the clusterization occurs. It leads to a significant drop in the x-ray signal since the cluster density decreases as well. Further experiments are currently under progress to provide more refined data which should allow quantitative comparison with atomic and solid targets.

7. Conclusion and perspectives

X-ray spectroscopy techniques have been used to investigate the collision dynamics of slow ($v < 1$ a.u) ions with different types of targets: atoms but also more complex systems as thin solids and clusters. More precisely, we have started to study the interaction of 255 keV Ar^{17+} ions with isolated atoms (Ar and N_2) provided by an effusive jet, with thin (10 and 80 nm) solid carbon foils and with clusters in a supersonic jet. Absolute x-ray emission probabilities have been measured. This probability is found much smaller with solids than in ion-atom collisions. With the supersonic cluster jet, the total x-ray signal is measured as a function of the backing pressure (P_0) in the production system. Preliminary results show a strong decrease of the signal with P_0 which can be attributed to the presence of clusters in the jet. Keeping in mind that aggregation is favored when increasing P_0, this tendency can be understood. Nevertheless, further data and analysis are needed to reach more quantitative comparison.

Finally, using a high resolution Bragg spectrometer, we have observed the complete series of Ar^{16+} $1snp\ ^1P_1 \rightarrow 1s^2$ transitions from $n = 2$ to 10 produced with free atoms while $K^1L^x \rightarrow K^2L^{x-1}$ transitions from Ar^{q+} excited ions with $1 \leq x \leq 8$ are generated with a thin solid foil. In the future, we intend to make high resolution x-ray spectroscopy with the cluster jet including coincidence measurements (X-ray emission with projectile ion charge state and energy loss).

References

[1] Krasnopolsky V A, Greenwood J B and Stancil P C 2004 *Space Sci. Rev.* **113** 271–373
[2] Aumayr F, Facsko S, El-Said A S, Trautmann C and Schleberger M 2011 *J. Phys.: Condens. Matter* 23 393001
[3] Trassinelli M, Gafton V E, Eddrief M, Etgens V H, Lacaze E, Lamour E, Luo X, Hidki S, Marangolo M, Mérot J, Prigent C, Reuschl R, Rozet J P, Steydli S, Vernhet D 2013 *Nucl. Instrum. and Methods B* in press
[4] Lemell C, Burgdörfer J, Aumayr F 2013 accepted in *Progress in Surface Science*
[5] Janev R K and Winter H 1985 *Phys. Rep.* **117** 265–387
[6] Ali R, Cocke C L, Raphaelian M L A and Stockli M 1994 *Phys. Rev.* A **49** 3586
[7] Tawara H, Richard P, Safronova U I and Stancil P C 2001 *Phys. Rev.* A **64** 042712
[8] Folkerts L and Morgenstern R 1990 *Europhys. Lett.* **13** 377
[9] Winecki S, Cocke C L, Fry Dand Stöckli M P 1996 *Phys. Rev.* A **53** 4228
[10] Winecki S, Stöckli M P, and Cocke C L 1997 *Phys. Rev.* A **56** 538
[11] Stöckl J, Suta T, Ditroi F, Winter H P and Aumayr F 2004 *Phys. Rev. Lett.* **93** 263201
[12] Burgdörfer J, Reinhold C, Meyer F 1995 *Nucl. Instrum. and Methods B* **98** 415
[13] Suto K and Kagawa T *Phys. Rev. A* 1998 **58** 5004 and *Phys. Rev. A* **63** 019903 (E)
[14] Trassinelli M, Prigent P, Lamour E, Mezdariz F, Mérot J, Reuschl R, Rozet J-P, Steydli S and Vernhet D 2012 *J. Phys. B* **45** 085202
[15] Briand J P, Giardino G, Borsoni G, Froment M, Eddrief M, Sébenne C, Bardin S, Schneider D, Khemliche H, Xie Z and Prior M 1996 *Phys. Rev. A* **54** 4136
[16] Briand J P and Benhachoum M 2009 *Nucl. Instr. and Methods* B **267** 665
[17] Martin S, Chen L, Brédy R, Bernard J, Salmoun A and Wei B 2004 *Phys. Rev. A* **91** 043202
[18] Manil B, Maunoury L, Huber B A, Jensen J, Schmidt H T, Zettergren H, Cederquist H, Tomita S and Hvelplund P 2003 *Phys. Rev. Lett.* **91** 215504
[19] Tappe W, Flesch R, Rühl E, Hoekstra R and Schlathölter T 2002 *Phys. Rev. Lett.* **88** 143401

[20] Prigent C, Lamour E, Mérot J, Pascal B, Rozet J-P, Trassinelli M, Vernhet D, Pacquet J-Y, Maunoury L, Noury F, RamillonJ-M 2009 *J. Phys. : Conf. Ser.* **163** 012111
[21] Lamour E, Prigent C, Eberhardt B, Rozet J P and Vernhet D 2009 *Rev. Sci. Instrum.* **80** 023103
[22] Giordmaine J A and Wang T C 1960 Molecular beam formation by long parallel tubes *J. Appl. Phys.* **31** 463
[23] Gray D C and Sawin H H 1992 *J. Vac. Sci. Technol.* A **10** 3229–38
[24] Rugamas F, Roundy D, Mikaelian G, Vitug G, Rudner M, Shih J, Smith D, Segura J and Khakoo M A 2000 *Meas. Sci. Technol.* **11** 1750
[25] Robertson J O'Reilly E P 1989 *Phys. Rev. B* **35** 2946
[26] Ziegler J-F, Biersack J-P, Ziegler M-D, Stopping and Range of Ions in Matter 2008 **293** SRIM Company
[27] Schenkel T, Hamza A V, Barnes A V, and Schneider D-H 1997 *Phys. Rev. A* **56** R1701
[28] Herrmann R, Cocke C L, Ullrich J, Hagmann S, Stoeckli M and Schmidt-Boecking H 1994 *Phys. Rev. A* **50** 1435
[29] Schwentner N, Himpsel F J, Saile V, Skibowski M and Steinmann W 1975 *Phys. Rev. Lett.* **34** 528
[30] Hagena O F 1991 *Rev. Sci. Instrum* **62** 2038
[31] M Trassinelli, C Ramond, E Lamour, J Mérot, C Prigent, J-P Rozet, S Steydli and D Vernhet 2012 J. Phys.: Conf. Ser. **388** 082009
[32] Salehzadeh A and Kirchner T 2013 *J. Phys. B* **46** 025201